Crystal structure and magnetic behaviour of nanocrystalline Fe-Nb-Cu-Si-B alloys studied by means of *in situ* neutron diffraction

1998 J. Phys.: Condens. Matter 10 5027

(http://iopscience.iop.org/0953-8984/10/23/009)

J. Phys.: Condens. Matter **10** (1998) 5027–5038. Printed in the UK PII: S0953-8984(98)91780-5

Crystal structure and magnetic behaviour of nanocrystalline Fe–Nb–Cu–Si–B alloys studied by means of *in situ* neutron diffraction

L Fernández Barquín†, J C Gómez Sal†, P Gorria‡§, J S Garitaonandia‡ and J M Barandiarán‡

† CITIMAC, Facultad de Ciencias, Universidad del Cantabria, Santander 39005, Spain
‡ Departamento de Electricidad y Electrónica, Facultad de Ciencias, Universidad del País Vasco, Bilbao 48080, Spain
§ Departamento de Física, Universidad del Oviedo, Oviedo 33007, Spain

Received 11 February 1998, in final form 19 March 1998

Abstract. Two Fe–Nb–Cu–Si–B alloys, $Fe_{73.5}Nb_3Cu_1Si_{13.5}B_9$ (B9) and $Fe_{77}Nb_4Cu_1Si_{12}B_6$ (B6), prepared with the ^{11}B isotope, have been analysed using data obtained by means of *in situ* neutron diffraction. This technique allows one to scrutinize crystallographic phases during thermal treatments, avoiding problems due to sample handling. The B9 sample develops Fe(Si) $Fm\bar{3}m$ (DO_3) nanometric crystals (10 nm) with 19 at.% Si in the phase when it is annealed at 500 °C for one hour. An increase to 800 °C favours the growth of Fe(Si) grains and the crystallization of other phases, mostly Fe borides. A Rietveld analysis of these phases results in a good reproduction of the nominal composition of the alloy. It also elucidates the crystallographic structure of the Fe(Si) phase. This is similar to the Fe_3Si $Fm\bar{3}m$ structure, but with some of the Fe atoms occupying some (45%) of the Si 4a sites. The compositions and amounts of the phases derived are in agreement with Mössbauer spectroscopy results for the same sample. Knowledge of the Fe(Si) composition enables one to compare the different magnetic behaviours observed for bulk and nanocrystalline alloys. By contrast, B6 alloy does not show the presence of a Fe(Si) DO_3 structure, presumably due to the lower amount of Si in the Fe(Si) phase. The thermal expansion of the phases that appear is fairly linear and the corresponding thermal expansion coefficients for the different phases have been extracted. The magnetic structure of the Fe(Si) phase is ferromagnetic collinear, without any trace of antiferromagnetic ordering. The thermal variation of the (1, 1, 1) magnetic peak intensity of the Fe(Si) phase matches well with reported DC magnetization results.

1. Introduction

Nanocrystalline alloys obtained by means of thermal treatments of amorphous compounds of Fe–Nb–Cu–Si–B [1–4] and Fe–Zr–B [5, 6] have given rise to a vast field of magnetism research recently, due to their outstanding magnetic properties. It has taken some time to characterize them magnetically and structurally, as they can be produced in different ways [1, 7, 8]. Probably due to their rather complicated composition, there was an early set of studies in which researchers attempted to improve their magnetic properties by slightly varying their composition [9–12]. Nowadays, it could be said that the usual production methods involve the annealing of amorphous samples at fixed temperatures and that the compositional research is nearly complete. However, a precise determination of their crystallographic structures and the relationship of these with the magnetic properties is still a subject of relevant interest.

0953-8984/98/235027+12$19.50

Excellent studies which attempted to characterize the Fe–Nb–Cu–Si–B alloys structurally [13–15] have established the existence of a Fe(Si) nanocrystalline phase that is produced upon annealing at low temperatures (typically 500 °C, for one hour), giving rise to some improved magnetic properties. These studies also show a subsequent onset of Fe borides at higher temperatures. It is generally accepted that nanocrystalline Fe(Si) has a DO_3 structure, similar to that of intermetallic Fe_3Si, but with some of the 4a Si sites randomly occupied by Fe atoms. At around 800 °C, as mentioned earlier, different iron borides precipitate and the Fe(Si) phase is no longer of nanometre size due to the crystal growth; this leads to a degradation of the attractive magnetic properties. In spite of these important conclusions, most of the studies have been performed mainly by means of Mössbauer spectroscopy and x-ray diffraction at room temperature on samples which had been previously prepared by appropriate annealing. This could be the origin of some of the uncertainties in the evaluation of such quantities as the composition of the phase, the crystal size and the roles of other phases, which have a tremendous influence on the macroscopic magnetic properties. This drawback is of some importance when one is trying to extract fine details of the crystallographic structure, but it can fortunately be overcome by using fast-data-collection diffraction techniques, which allow *in situ* experiments to be carried out, using modern high-flux synchrotron and neutron sources. X-ray sources probably provide the quickest pattern-collection times and are better suited for kinetic analyses, especially for phenomena occurring on the sample surface. On the other hand, neutron diffraction, as is well known, allows the identification and scanning of crystal phases grown in the bulk alloy, including their magnetic structures. It turns out to be the case that most of the crystalline phases appearing during the nanocrystallization (and further crystallization) processes are magnetic, reinforcing strongly the need for careful neutron diffraction studies of the above-mentioned alloys.

In this article, we have concentrated our attention on the 'standard' FINEMET composition $Fe_{73.5}Nb_3Cu_1Si_{13.5}B_9$, for which there has been most discussion of magnetic results [1, 2 13–15]. Also, for the purposes of some timely comparison, there has been some analysis of a $Fe_{77}Nb_4Cu_1Si_{12}B_6$ alloy, as described below. Apart from the usual size determination of the crystals, study of the growth rate etc, for the nanocrystalline state a complete structural and magnetic refinement has been performed on the fully crystallized samples by Rietveld analysis. This compares calculated theoretical diffraction patterns to the experimental data, allowing the fitting of diverse sets of crystallographic parameters to be performed.

2. Experimental procedure and data analysis

Amorphous alloys of $Fe_{73.5}Nb_3Cu_1Si_{13.5}B_9$ (B9) and $Fe_{77}Nb_4Cu_1Si_{12}B_6$ (B6) were melt spun into ribbon shapes. Enriched boron, ^{11}B (98%), was used in the master alloys to avoid severe neutron absorption. Amorphous samples were checked by x-ray (Cu Kα) diffraction (XRD). Furthermore, and in order to compare these ribbons in their initial forms to the ones containing natural boron, differential scanning calorimetry (DSC), XRD and Mössbauer spectroscopy measurements were carried out. The results are very similar for the two types of sample. A ^{57}Co–Rh source was employed in the Mössbauer spectroscopy; further details and the fitting programs used to analyse the spectra were recently given elsewhere [15].

The neutron diffraction experiments were carried out using the D1B instrument at the Institute Laue–Langevin (ILL) at Grenoble. Diffractograms were recorded between 32.9° and 112.7° (2θ) and the neutron wavelength was 2.5219 Å. The samples (about 2 g) were placed in thin vanadium cylinders and heated up in a furnace under vacuum. The temperature

control was effected by thermocouples close to the sample. For the B9 sample, the thermal treatment was as follows: it was heated from the amorphous state to 500 °C, annealed at that temperature for two hours, subsequently warmed to 800 °C and then annealed (for one hour) at that temperature. Afterwards, one-hour patterns were recorded between 800 °C and 225 °C (at 800, 700, 600, 500, 400, 300 and 225 °C) for the fully crystallized sample. Neutron diffraction patterns were recorded approximately every ten minutes during the thermal treatment. Neutron patterns were also recorded for a fully crystallized B6 sample, at 200, 300, 400, 500, 600, 670 and 800 °C.

Crystallographic analyses of the magnetic and nuclear structure of the phases that appeared were performed by Rietveld analysis [16] using the FULLPROF code [17] (the freeware program was kindly supplied by Dr J Rodríguez Carvajal (Laboratoire Leon-Brillouin)). The conventional Rietveld indices, such as the Bragg (R_B), expected (R_{exp}), profile (R_p) and weighted-profile (R_{wp}) indices, are defined as usual (see reference [17]). The initial crystallographic parameters for the crystal phases tested were extracted from *Pearson's Handbook* [18].

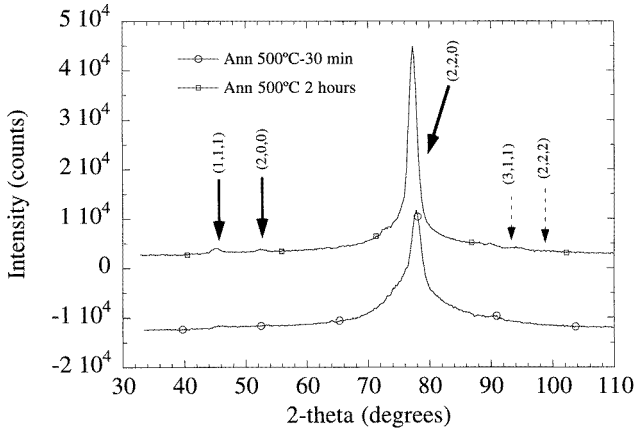

Figure 1. Neutron spectra of B9 after 30 minutes or two hours at 500 °C. The '30 min' pattern has been shifted down for clarity. The positions of the peaks of the Fe(Si) $Fm\bar{3}m$ structure are marked with arrows. The (3, 1, 1) and (2, 2, 2) peak positions (indicated by dashed arrows) are still swamped by the background.

3. The crystallization process of FINEMET alloys

3.1. The onset and isothermal evolution of the magnetic Fe(Si) nanosized structure

Figure 1 shows the neutron spectra obtained after half an hour and after two hours at 500 °C. This latter pattern clearly shows three peaks (at around 44.5°, 52.5° and 77°) superposed on a still relatively large amorphous contribution. It is worth noticing the appearance of the two lower-angle peaks, which correspond to the (1, 1, 1) and (2, 0, 0) reflections of an Fe(Si) cubic $Fm\bar{3}m$ structure, known as DO_3. The remaining amorphous contribution masks the expected (3, 1, 1) and (2, 2, 2) peaks of that structure. The evolution of the intensities, widths and positions of the diffraction peaks during this annealing process has been analysed using Gaussian functions for peak fittings (in the case of the (2, 2, 0) peak at around 77°, another Gaussian for the large amorphous background was also included). In

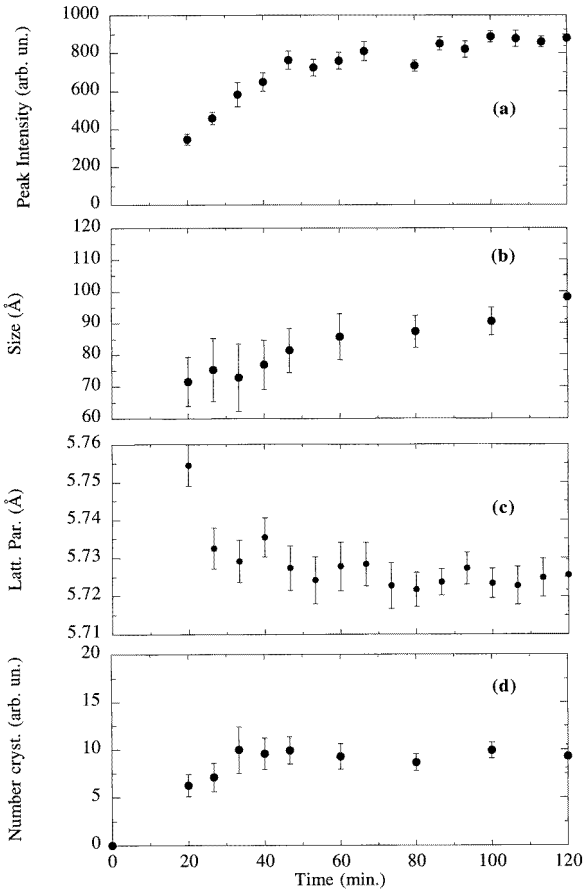

Figure 2. The time variation of the intensity (a) and grain size (b) (both deduced from the Fe(Si) (1, 1, 1) peak), and of the lattice parameter (c) of the Fe(Si) phase at 500 °C. Panel (d) shows the time evolution of the number of crystals (see the text).

figure 2, the time evolutions of integrated intensity (proportional to the amount of crystal present) (figure 2(a)) and the crystal size deduced from the peak width using the Scherrer formula (figure 2(b)) are depicted. Both data sets have been extracted from the analysis of the (1, 1, 1) peak, in which the amorphous contribution should be less prominent. The lattice parameter variation with time, calculated by the $\cos\theta\cot\theta$ method [19], is also presented (figure 2(c)). The strongest variation takes place during the first hour for all three parameters. It appears that the crystallographic phase formed has become fairly well established in this time and the magnetic properties of this crystallographic phase related to the structural arrangements remain fairly stable subsequently. Hence, the crystal size increases only to a certain saturation value, around 10 nm; this is the origin of the special soft-magnetic properties of these alloys [1–3]. The saturation of the crystal size growth (figure 2(b)) and the peak intensity (figure 2(a)) at about 80 min suggests a common origin. An estimation of the number of crystallites at a given time can be obtained by dividing the amount of crystalline phase (proportional to the peak intensity) by the average volume of the grains (proportional to the third power of the grain size). That quantity is represented in figure 2(d). After a rapid growth, the number of crystals remains constant and the increase

of the amount of crystalline phase present is then only due to crystal growth. This behaviour is as expected for a heterogeneous nucleation, at the Cu-rich sites, and for growth which is slowing down due to the very different diffusion coefficients of the atomic species involved in the primary crystallization (Fe, Si, Nb, B) [20]. Previously, such results have only been deduced from RT measurements after annealings for different times and at different temperatures; ours come from a direct study of the nanocrystallization kinetics, with the data obtained *in situ* during the process.

Table 1. Crystallographic parameters deduced from Rietveld fittings for the FINEMET (B9) sample at 800 °C. R_B: the Bragg factor. Thermal coefficient: $\alpha = (1/L)(\Delta L/\Delta T)$. The errors in the parameters are given in brackets. Conventional Rietveld factors defined in reference [17]: $R_p = 20.2$; $R_{wp} = 22.3$; $R_{exp} = 1.05$.

Phase	R_B (%)	Amount (%)	Lattice parameter (Å)	Thermal coefficient (10^{-5} K^{-1})	Space group
Fe(Si)	1.6	46	$a = 5.771(1)$	1.77(6)	$Fm\bar{3}m$
Fe_2B	18.1	11	$a, b = 5.167(2)$	1.15(5)	$I4/mcm$
			$c = 4.278(2)$	1.20(9)	
Fe_3B	26.8	14	$a = 5.390(3)$	1.34(6)	$Pnma$
			$b = 6.786(4)$	1.70(2)	
			$c = 4.547(3)$	1.03(5)	
$Fe_{23}B_6$	25.8	1	$a = 10.920(10)$	0.95(22)	$Fm\bar{3}m$
Nb_5Si_3	38.8	6	$a = 6.656(16)$	1.44(20)	$I4/mcm$
			$c = 11.729(7)$	1.16(3)	
Fe_2Si	8.4	22	$a = 3.977(19)$	1.73(5)	$P\bar{3}m1$
			$b = 5.240(19)$	1.02(6)	

On the other hand, the saturation value for the Fe(Si) cubic lattice parameter is around 5.726(6) Å, this value being obtained at high temperature (500 °C). Unfortunately, a Rietveld refinement is not advisable in this case, due to the poor degree of crystallization of the samples at this stage. An estimation of the lattice parameter at room temperature could be obtained by considering the linear expansion coefficient ($\alpha = (1/L)\Delta L/\Delta T = 1.77 \times 10^{-5}$ K^{-1}) of the fully crystallized Fe(Si) phase, as deduced in section 3.2 and presented in table 1. The RT value for the lattice parameter is then 5.675(11) Å, which is slightly lower than the value corresponding to a fully crystallized sample (5.690(11) Å), this difference presumably being due to the existence of internal stresses in the nanocrystalline phase. Using well known tables from references [21, 22], which relate the lattice parameter to the atomic percentage of Si present, we found that our value corresponds to an 18.8(1.2)% Si content in the Fe(Si) phase. This value is the same as the one obtained from the lattice parameter extracted from an XRD study of commercial FINEMET samples annealed at 500 °C with the measurements made at room temperature and recent Mössbauer results; these indicate a percentage of Si of around 18.8(2)% [15]. Therefore, the neutron results for the annealing process at 500 °C can be summarized as follows:

(i) the nanocrystalline Fe(Si) phase is fairly stable after one hour of initial growth; and
(ii) the amount of Si in the established nanocrystalline phase is around 19%.

The difference between the magnetic properties of the nanocrystalline phase and those for the bulk alloys can be assessed from the values of the Curie temperatures: from reference [23], the Curie temperature for a 19 at.% Si bulk alloy should be around 637 °C. This value estimated from the above analysis is far from the value actually obtained from magnetization

data for a nanocrystalline alloy (580 °C), confirming earlier suggestions by Gorria and co-workers [15, 24] of the variation of magnetic properties of nanocrystals caused by changes in size, interaction with the amorphous phase and interactions due to crystal imperfections.

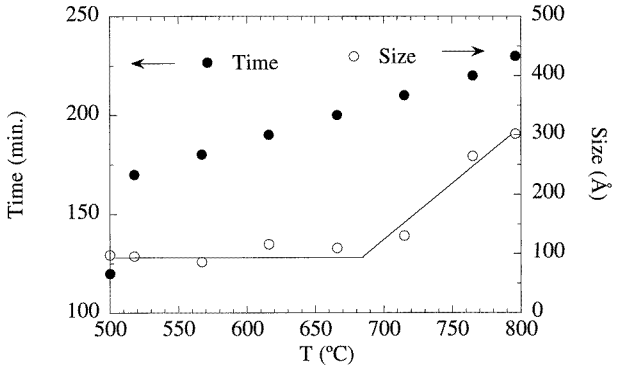

Figure 3. The variation in grain size with increasing temperature (right-hand scale, open circles) and time (left-hand scale, full circles) during the heating process and after the two-hour annealing at 500 °C. Note the difference between the first two time points due to the furnace lag.

3.2. Final crystallization: the appearance of magnetic Fe borides

Further temperature increase from 500 °C to 800 °C for about two hours results in:

(i) a decrease of the amorphous contribution;
(ii) a size enlargement of the Fe(Si) nanocrystals described in the previous section; and
(iii) crystallization of Fe borides.

The variation of grain size for the Fe(Si) phase during this process (see figure 3) shows a sharp transition at around $T = 680$ °C. At that temperature, clearly the nanocrystals of Fe(Si) start growing, which corresponds to the second crystallization step [15, 25]. At 800 °C, the alloy is totally crystallized and the diffraction peaks are rather sharp, as shown in figure 4.

The large number of initial elements in the amorphous alloy is the origin of the appearance of the numerous phases that are eventually analysed by the Rietveld method. In fact, great care should be taken not to incorporate spurious phases into the fitting procedure. Also, the magnetic character of some of the phases can introduce extra difficulty. In our case, we opted to analyse first the highest-temperature pattern (800 °C), for which magnetic order is absent and the spectra can only be of nuclear origin, as is deduced from magnetization data [15]. In addition, bearing in mind previous results [13–15], several expected phases were included in the analysis, such as Fe(Si) $Fm\bar{3}m$, Fe_2B $I4/mcm$ and Fe_3B $Pnma$; these expected phases in fact represented more than 70% of the peak intensity of the pattern (see table 1) for B9. Also, similar phases can be used to reproduce the majority of the spectrum for the B6 sample. The pattern shown in figure 4 has been analysed assuming the above-mentioned phases to be present. In order to account for the experimental pattern, three supplementary ones have also been included: $Fe_{23}B_6$ $Fm\bar{3}m$, Nb_5Si_3 $I4/mcm$ and Fe_2Si $P\bar{3}m1$. With all of these phases included, the agreement is excellent and the pattern is solved. In figure 5, an enlargement of the central angular range of the pattern is shown. In this figure the most significant features that led us to consider the above-mentioned phases

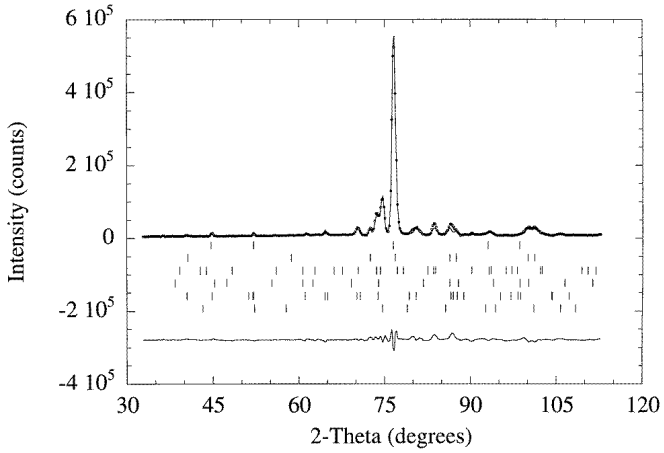

Figure 4. The neutron pattern of the B9 sample at 800 °C (points). Also shown are the spectra fitted by Rietveld calculation (line) and the difference (bottom line) between the calculated and experimental patterns. The vertical lines mark the peak positions for the phases (from top to bottom): Fe(Si), Fe_2B, Fe_3B, $Fe_{23}B_6$, Nb_5Si_3 and Fe_2Si.

can be seen: the main peak at $\cong 77^\circ$ is mainly accounted for by the (2, 2, 0) reflection of the Fe(Si) phase; Fe_2B contributes to the peaks at $\cong 72.5^\circ$, (0, 0, 2), and 87°, (1, 1, 2) and (2, 2, 0), among others, whereas the presence of the Fe_3B phase explains the intensity at around 84° (1, 3, 1); the peaks close to 75° and 80° are accounted for by the (1, 0, 2) Fe_2Si and the (0, 0, 6) Nb_5Si_3 reflections, respectively.

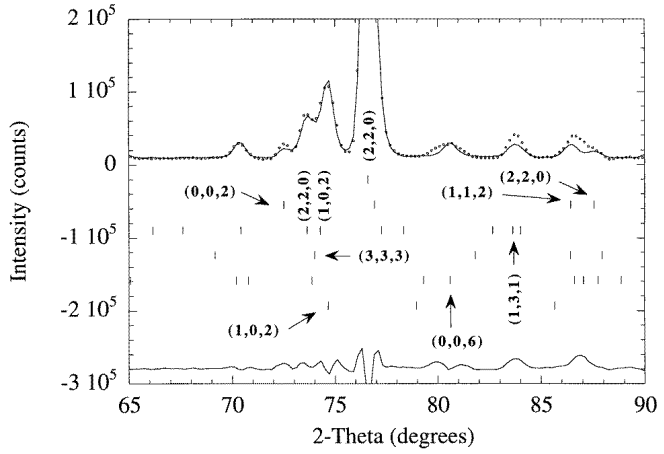

Figure 5. An enlarged neutron pattern of the B9 sample at 800 °C (points), presented to clarify the correspondence between the diffraction peaks and the proposed phases. The arrangement is the same as in figure 4: the vertical lines correspond, from top to bottom, to Fe(Si), Fe_2B, Fe_3B, $Fe_{23}B_6$, Nb_5Si_3 and Fe_2Si. Some of the most characteristic reflections have been labelled.

The crucial point is the defining of the crystallographic parameters of the Fe(Si) phase in the pattern. This was not possible in a previous study using samples similar to the present ones, due to the sparser statistics of the recorded neutron patterns [26]. However, and as

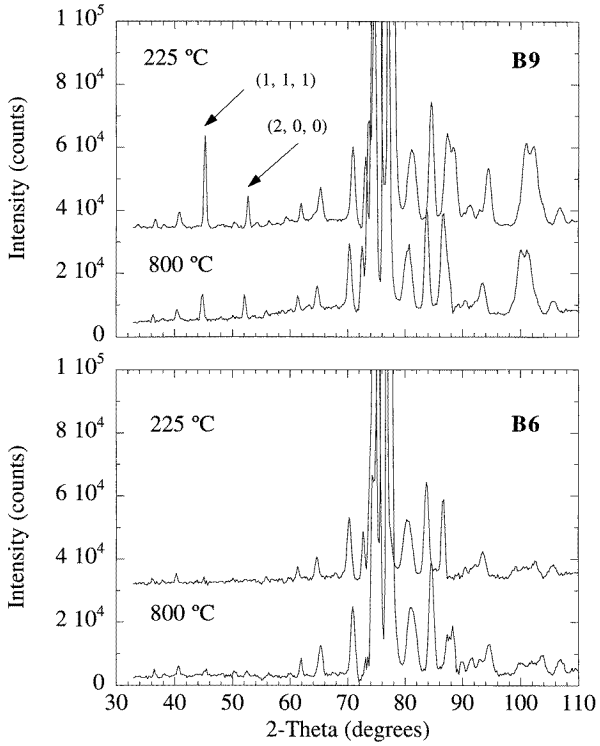

Figure 6. The neutron patterns of fully crystallized B6 and B9 at the highest two temperatures. The reduced scales enable us to observe clearly the variation of the intensity for the B9 sample of the (1, 1, 1) and (2, 0, 0) peaks of Fe(Si) $Fm\bar{3}m$. The angular shift of the peak positions is caused by thermal expansion.

has been described in the previous section, the clear peaks appearing at around 44.5°, 52° and 77° for B9 are signs of the existence of an ordered Fe(Si) phase (DO_3 structure). This is not the case for B6, for which such peaks are absent (see figure 6), thus indicating the existence of a bcc Fe(Si) phase with Si atoms distributed at random at all of the sites. This change is expected from the difference in Si content of the two phases (about 19% in the Fe(Si) phase for B9 and 10% in the bcc Fe(Si) phase for B6); the transition from a solid solution at low Si content to a DO_3 structure at high Si content occurs at around 10% of Si [22]. For B9, a Fe(Si) phase can be described directly by taking the atomic positions of Fe_3Si together with a random distribution of Fe and Si atoms at the 4a sites of the $Fm\bar{3}m$ structure. In fact, the best fit is obtained when around 45(10)% of the atoms at such sites are Fe atoms, giving a composition for this phase such as $Fe_{3.45}Si_{0.55}$ and a total percentage of Si in the phase of around 13.8(2.5)%. In addition, the percentage of Si in the Fe(Si) phase is in good agreement with the result extracted from the analysis of the lattice parameter: this is 5.771(1) Å at 800 °C. By considering the thermal variation of the lattice parameters obtained from lower-temperature spectra, given in table 1, it is possible to perform an extrapolation to RT, yielding a value of around 5.693(18) Å. From conversion tables again, that value corresponds to 15.4(3.5)% of Si in the Fe(Si). An obvious objection should be raised at this point: the amount of Si is different here from the predictions of other techniques. Values for the Si content in Fe(Si) of around 17–18% have been reported

from XRD studies [13, 14] and Mössbauer spectroscopy gives 17% for this sample (see figure 7). The variation in the percentages given in different reports are to be expected due to: the use of different techniques; samples with slight variation in actual composition; and the inherent lack of accuracy due to the large number of phases involved in the respective analyses. Here, (i) the *in situ* character of the present neutron results and (ii) the fact that the lattice parameter analysis and the Rietveld occupancy of Si at the 4a sites produce similar values support the consistency of the present results.

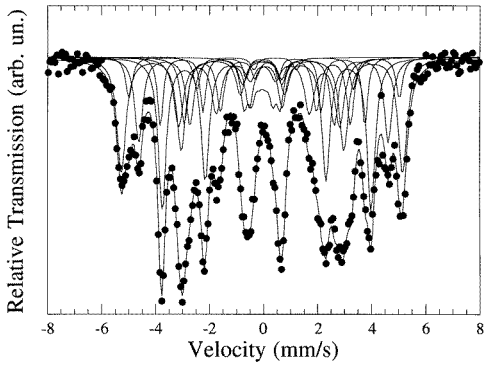

Figure 7. The Mössbauer spectrum of fully crystallized B9 at RT. The fits correspond to Fe(Si), Fe_2B, $Fe_{23}B_6$ and Fe–Nb–B. The fitting details are the same as those explained in reference [15].

As regards the rest of the phases (see table 1), Rietveld fits including iron boride (Fe_2B, Fe_3B and $Fe_{23}B_6$) phases give reasonably low Bragg factors (<30%) in the analysis of the crystallized amorphous samples [27]. The presence of these phases has been indicated by previous Mössbauer results [13–15], and this is also the case for the Mössbauer spectrum obtained for the B^{11} samples studied here, shown in figure 7. As can be observed in figures 5 and 6, most of the peak contributions lie in an angular interval from 70° to 90°, which further increases the difficulty of assigning these peaks. A final definitive improvement comes from the addition of Nb_5Si_3 ($I4/mcm$) and Fe_2Si ($Pm\bar{3}1$) phases in the theoretical pattern. The first one accounts for the Nb existing in the original amorphous alloy. Among the possible phases including Nb, Nb_5Si_3 provides the best result, which, in addition, gives a reasonable final percentage of Nb (3.8%) in the alloy. Other phases such as Fe–Nb or Fe–Nb–B have also been suggested [13–15]; however, they do not account for the remaining intensity of the spectra, even with distorted/preferred orientations. On the other hand, the pattern is successfully fitted using Fe_2Si. This phase is evident in the spectrum at 800 °C, corroborating the assertion that it is normally found at high temperatures, but it even appears at room temperature in our sample. This should not be considered strange for these FINEMET alloys, as crystallization can produce distorted structures of small size, so it is entirely possible for high-temperature phases to become stabilized on decreasing the temperature. It should also be recalled that this Fe_2Si phase increases the total amount of Si in the Fe–Si phases to around 13.7% (see table 1). This ties in with the previous discussion of the Si percentage in the Fe(Si) phase. It seems that neutron diffraction distinguishes between Fe(Si) DO_3 and another Fe–Si phase (distorted Fe_2Si), which combined provide the real Si percentage, which is closer to that obtained from Mössbauer studies (figure 7)—about 17%. Moreover, the proposed amounts of the six respective phases lead to the following predictions for the percentages of elements that should be present: Fe: 73%, Si: 13.7%, Nb: 3.8% and B: 7.4%; this matches the nominal composition of the alloy well, which is

further evidence in favour of the presence of the proposed phases. Again, a thorough search for phases has been performed in the literature, but only the above-mentioned phases gave satisfactory results. A possible contribution from Cu $Fm\bar{3}m$ has been disregarded due to its low percentage and to the fact that its diffraction peaks are masked by those due to other phases.

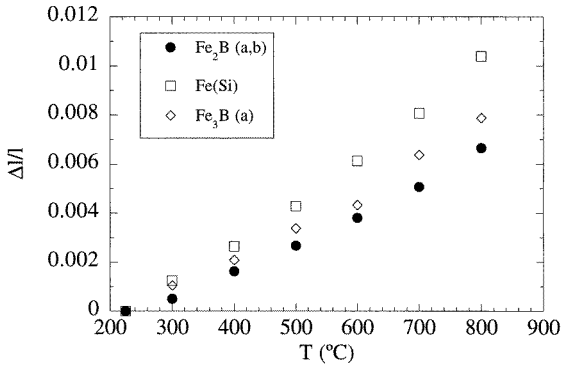

Figure 8. The thermal expansion of the lattice parameter a for some of the most characteristic crystalline phases in the FINEMET B9 alloy. The variation is fairly linear over the range studied. The lattice parameter c for Fe_2B has been missed out for clarity.

Once the 800 °C diagram is solved (figure 4), an investigation of the temperature variation of the lattice parameters during the process of cooling to lower temperatures provides the thermal expansion coefficients for all of the phases included. The thermal expansions of the proposed phases present fairly linear behaviour for B9 over the temperature range studied (see figure 8), and the values (which are close to those for the B6 sample) have been included in table 1. The value of the thermal expansion for Fe(Si) has been already used in the previous discussion of the percentage of Si in the above-mentioned phase. It should be noted that this value is higher than that reported for pure Fe $Im\bar{3}m$ (1.21×10^{-5} K^{-1}) [23].

4. The thermal behaviours of the magnetic structures of the crystallized products

In figure 6, the patterns at 800 °C and 225 °C for B9 and at 200 °C for B6 are depicted for the fully crystallized samples. There is a global decay of the peak intensity with increasing temperature and there are no new peaks in the lower-temperature patterns. This is a clear sign of a ferromagnetic behaviour of the magnetic phases, without any visible antiferromagnetic contribution. For B6, the variations are subtle and practically impossible to evaluate. However, for B9, the intensity variation for the peak at 44.5°, which corresponds to Fe(Si) (1, 1, 1), is particularly readily observed. Bearing in mind the bulk magnetization results [15], it is expected that the Curie temperatures of the Fe(Si) phase ($T_C \cong 637$ °C) should be apparent in the intensity variation. A complete magnetic Rietveld refinement, including magnetic Fe borides (such as Fe_2B ($T_C = 742$ °C [28]), Fe_3B ($T_C = 527$ °C [29]), $Fe_{23}B_6$ ($T_C \approx 400$ °C [15])) is irrelevant for these multiphase crystallized alloys, because the observed peaks correspond in general to several phases present at small percentages.

Only the magnetic (1, 1, 1) and (2, 0, 0) peaks of the Fe(Si) phase allow an at least qualitative analysis. However, it is well known that for cubic compounds no indications as regards the magnetic moment direction can be extracted from powder neutron measurements;

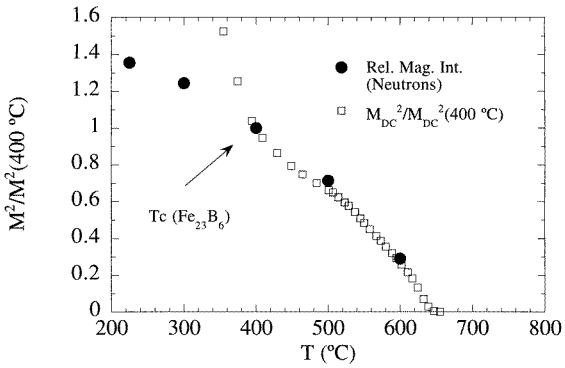

Figure 9. The thermal variation of the relative magnetic intensity of the Fe(Si) (1, 1, 1) peak scaled to match the squared DC magnetization (relative to that at 400 °C) for a fully crystallized commercial sample (the data were taken from reference [15]).

just the collinear ferromagnetic structure of the Fe(Si) can be ascertained. In addition, it is possible to scale the relative temperature variation of the magnetic peak intensity of the Fe(Si) (1, 1, 1) peak (better defined than that of the (2, 0, 0) one) to match the variation of $M^2_{DC}(T)$ for a commercial B9 sample [15] (see figure 9). It should be recalled that in this variation, contributions from Fe borides are superposed on that from the Fe(Si). In particular, the Curie temperature of $Fe_{23}B_6$ is observed to be around 400 °C. The variation obtained is similar to that of M^2_{DC} in the region between 400 °C and 670 °C. This is the region in which the magnetic behaviour is due solely to the Fe(Si) phase. Our neutron data permit us to define more precisely the behaviour at $T < 400$ °C for the Fe(Si) phase: the thermal variation becomes progressively saturated to lower temperatures. The agreement found between the results obtained from the two techniques is remarkable and lends further support to the present characterization of the nuclear and magnetic crystallographic structure of the Fe(Si) phase.

5. Conclusions

The use of neutron diffraction to analyse the structural and magnetic evolution of nanocrystalline alloys has resulted in a precise and direct evaluation of the formation of the nanocrystalline state, yielding valuable information about the amount, size and composition of the Fe(Si) nanocrystals. Also, Rietveld analyses of the fully crystallized samples have allowed us to define the percentages of the final phases and to carry out a crystallographic study of the Fe(Si) structure using a modified Fe_3Si structure including Fe atoms at the Si 4a sites. The presence of clear peaks permitted us to extract the amount of Si (19%) present in the nanometric phase which is formed in during the first 60 minutes of annealing at 500 °C. These results coincide with previous Mössbauer ones obtained for commercial samples and the ones presented here for ^{11}B samples. At higher temperatures, Fe borides are found together with Nb_5Si_3 and Fe_2Si. The variations of the magnetic intensity are signs of a ferromagnetic collinear state of the Fe(Si) phase. In particular, it has been possible to scale the thermal evolution of the magnetic intensity of the (1, 1, 1) peak of Fe(Si) to match the thermal variation of the magnetization obtained previously for similar alloys.

Acknowledgments

We thank the Spanish CICYT for financial support under grant MAT96-1023. We also thank the ILL staff for assistance during the experiments.

References

[1] Yoshizawa Y, Oguma S and Yamauchi K 1988 *J. Appl. Phys.* **64** 6044
[2] Herzer G 1990 *IEEE Trans. Magn.* **25** 3327
[3] Herzer G 1993 *Phys. Scr.* T **49** 307
[4] Chen C, Luan K Z, Liu Y H, Mei L M, Guo H Q, Shen B G and Zhao J G 1996 *Phys. Rev.* B **54** 6092
[5] Suzuki K, Makino A, Inoue A and Masumoto T 1991 *J. Appl. Phys.* **70** 6232
[6] Kopcewicz M, Grabias A, Nowicki P and Williamson D L 1996 *J. Appl. Phys.* **79** 993
[7] El Ghannami M, Kulik T, Hernando A, Fernández Barquín L, Gómez Sal J C, Gorria P and Barandiarán J M 1994 *J. Magn. Magn. Mater.* **133** 314
[8] Gorria P, Orúe I, Plazaola F and Barandiarán J M 1993 *J. Appl. Phys.* **73** 6600
[9] Randrianantoandro N, Slawska-Waniewska A and Greneche J M 1997 *Phys. Rev.* B **56** 10 797
[10] Frattini R, Mulas G, Enzo S and Cowlam N 1997 *Nanostruct. Mater.* **9** 513
[11] Liu X D, Lu K, Ding B Z, Hu Z Q, Zhu J and Jiang J 1994 *Physica* B **193** 147
[12] Mattern N, Danzig A and Müller M 1995 *Mater. Sci. Eng.* A **194** 77
[13] Hampel G, Pundt A and Hesse J 1992 *J. Phys.: Condens. Matter* **4** 3195
[14] Rixecker G, Schaaf P and Gonser U 1992 *J. Phys.: Condens. Matter* **4** 10 295
[15] Gorria P, Garitaonandia J S and Barandiarán J M 1996 *J. Phys.: Condens. Matter* **8** 5925
[16] Rietveld H M 1967 *Acta Crystallogr.* **22** 151
[17] Rodríguez Carvajal J 1990 *Satellite Mtg of the 15th Congr. of the International Union of Crystallography* (Toulouse: IUC) p 127
Rodríguez Carvajal J 1993 *Physica* B **192** 55
[18] Villars P and Calvert L D 1985 *Pearson's Handbook of Crystallographic Data for Intermediate Phases* (Cleveland, OH: American Society of Metals)
[19] Cullity B D 1960 *Elements of X-ray Diffraction* (New York: Addison-Wesley) p 330
[20] Hono K, Hiraga K, Wang Q, Inoue A and Sakurai T 1992 *Acta Metall. Mater.* **40** 2137
[21] Bozorth R 1951 *Ferromagnetism* (Princeton, NJ: Van Nostrand) p 74
[22] Kubachewski O 1982 *Iron Binary Phase Diagrams* (Berlin: Springer)
[23] Chin G Y and Wernick J H 1980 *Ferromagnetic Materials* vol II (New York: North-Holland) p 55
[24] Hernando A, Navarro I and Gorria P 1995 *Phys. Rev.* B **51** 3281
[25] Jiang J Z 1997 *Nanostruct. Mater.* **9** 245
[26] Fernández Barquín L, Gorria P, Barandiarán J M, Gómez Sal J C and Rodríguez Carvajal J 1997 *Physica* B **234–236** 418
[27] Fernández Barquín L, Barandiarán J M, Tellería I and Gómez Sal J C 1997 *Phys. Status Solidi* a **155** 439
[28] Murphy K A and Hershkowitz N 1973 *Phys. Rev.* B **7** 23
[29] Chien C L, Musser D, Gyorgy E M, Sherwood R C, Chen H S, Luborsky F E and Walter J L 1979 *Phys. Rev.* B **20** 283